Electronic Supplementary Material (ESI) for Journal of Materials Chemistry A.

Supporting Information

Double gradient composite dielectric with high energy density and efficiency

Yanan Shang [ab], Yu Feng *[ab], Changhai Zhang [ab], Tiandong Zhang [ab], Qingquan Lei [ab] and Qingguo Chi *[ab]

[a]*Key Laboratory of Engineering Dielectrics and Its Application, Ministry of Education, Harbin University of Science and Technology, Harbin 150080, PR China*

[b]*School of Electrical and Electronic Engineering, Harbin University of Science and Technology, Harbin 150080, PR China*

*Corresponding author: E-mail: fengyu@hrbust.edu.cn (Yu Feng);

qgchi@hotmail.com (Qingguo Chi).

Table S1. The composite parameters used in the simulation of this work.

Material	Dielectric constant	Breakdown strength (kV/mm)
Polymer	5.07	562.80
TiO_2	59.00	350.00
BNNS	3.00	1000.00

Part 1. Improvement of polymer matrix properties

In order to better apply PVDF based polymer to the field of energy storage, from the perspective of material optimization, a certain volume PMMA is blended with P(VDF-TrFE-CFE) to improve breakdown strength and charge-discharge efficiency of PVDF based polymer matrix. Pure P(VDF-TrFE-CFE) (recorded as 0:10), PMMA/P(VDF-TrFE-CFE) blend polymers with volume ratios of 1:9, 2:8, 3:7, 4:6 and pure PMMA (recorded as 10:0) were prepared respectively. The cross-section SEM images of each polymer is given in Fig.S1. SEM images show that the thickness of each polymer is almost the same (~15μm). The cross-section structure is smooth and complete without obvious holes and cracks, indicating that two kinds polymers have well compatibility.

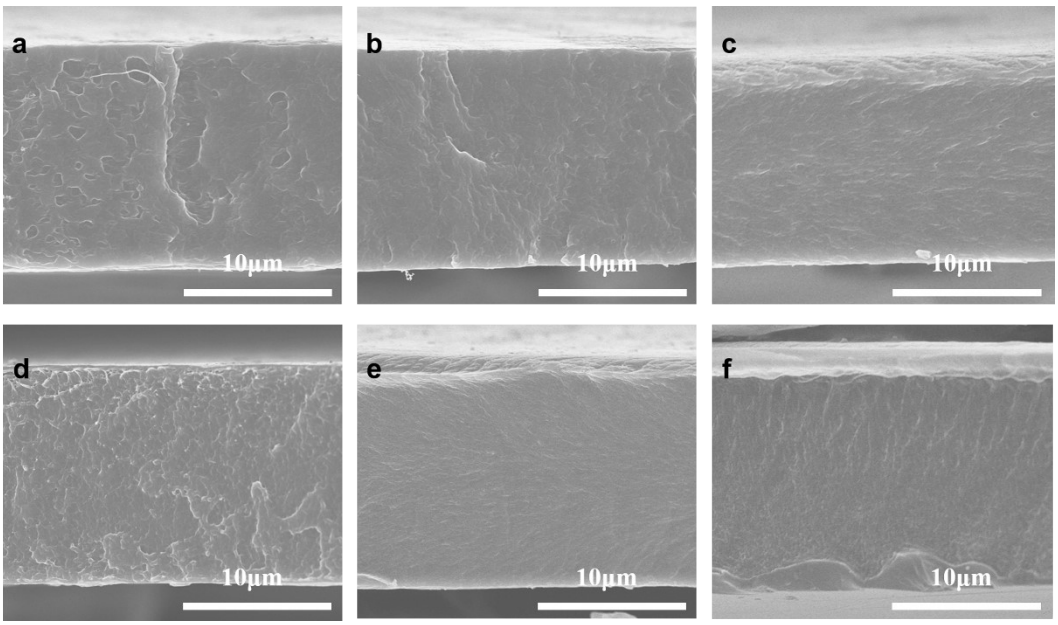

Fig.S1 Cross-section SEM images of a) Pure P(VDF-TrFE-CFE); PMMA/P(VDF-TrFE-CFE) blend polymers with volume ratios of b) 1:9; c) 2:8; d) 3:7; e) 4:6; f) Pure PMMA.

The XRD patterns of Fig.S2a can be observed that with the increasement of PMMA ratio, the characteristic peak of P(VDF-TrFE-CFE) at 2θ=18.2° and 2θ=20.1° is getting smaller, and the amorphous slow scattering peak (PMMA characteristic peak) gradually appears in the range at 2θ=13~18°. XRD results show that the content of PMMA have a significant effect on crystal form of PMMA/P(VDF-TrFE-CFE) blend polymers. Fig.S2b shows FTIR results of blend polymers.

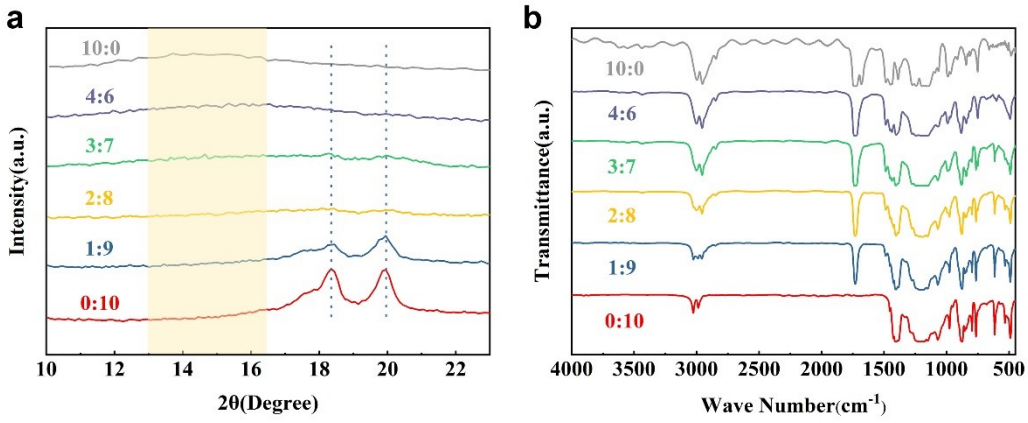

Fig.S2 a) The XRD patterns and b) FTIR spectra of blend polymers.

Fig.S3 is the DSC heating curve of blend polymers. It can be known from figure that with the

enhancement of PMMA content, the melting temperature of blended polymer gradually decreases, and the melting peak height is weakened. This is because the rigid PMMA molecular chain restricts the movement of P(VDF-TrFE-CFE) molecular chain. The crystallinity (χ_c) of introduced PMMA blend polymer can be calculated by the following formula:[1]

$$\chi_c = \frac{\Delta H_m}{(1\text{-}m_P)\Delta H_m^*} \times 100\%$$

where ΔH_m is normalized melting enthalpy; m_p is the weight percent of PMMA in polymer; ΔH_m^* is melting enthalpy of PVDF-based polymer at 100% crystallization (104.7 J/g).[2] The crystallinity calculation results are displayed in Table S2. It can be seen that PMMA reduces the crystallinity of P(VDF-TrFE-CFE), which will help to boost breakdown strength of blend polymers.

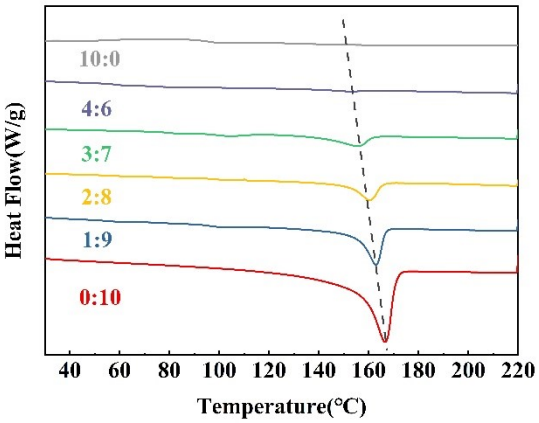

Fig.S3 DSC heating curve of blend polymers.

Table S2. Melting peak and crystallinity of blend polymers.

Polymer	P(VDF-TrFE-CFE)	1:9	2:8	3:7	4:6
Melting peak	166.08℃	163.48℃	160.94℃	157.97℃	152.66℃
Crystallinity	92.5%	35.2%	21.6%	6.5%	1.8%

Fig.S4a shows the variation of dielectric constant and dielectric loss with frequency for pure P(VDF-TrFE-CFE), PMMA/P(VDF-TrFE-CFE) blend polymers and pure PMMA. The dielectric

constant of pure P(VDF-TrFE-CFE) is higher than that of pure PMMA and polymer blends in the whole frequency range. And with the increasement of PMMA content, dielectric constant gradually decreases, but all larger than pure PMMA. It can be attributed to two aspects: one is that PMMA has a lower dielectric constant; the other is that PMMA reduces the crystallinity of P(VDF-TrFE-CFE). The dielectric loss of pure P(VDF-TrFE-CFE) shows a trend of first decreasing and then increasing with the augment of frequency. This is because the dipole turning cannot follow the variation of frequency, so that the dipole turning cannot recover in time, leading to enlarged loss. However, the introduction of PMMA effectively restricted molecular chain movement and dipole mobility of P(VDF-TrFE-CFE), and significantly suppressed dielectric loss at high frequency. The leakage current test in Fig.S4b also shows that after introduction of PMMA, the conduction loss of polymer is significantly restricted, which will help boost charge-discharge efficiency and breakdown field strength of composite dielectric. Fig.S4c shows the frequency dependence of dielectric constant and dielectric loss of blend polymers under a bias field of 100 kV/mm. It can be observed that in frequency range of 10^2~10^5 Hz, dielectric constant and dielectric loss value varies little with frequency, maintaining good stability.

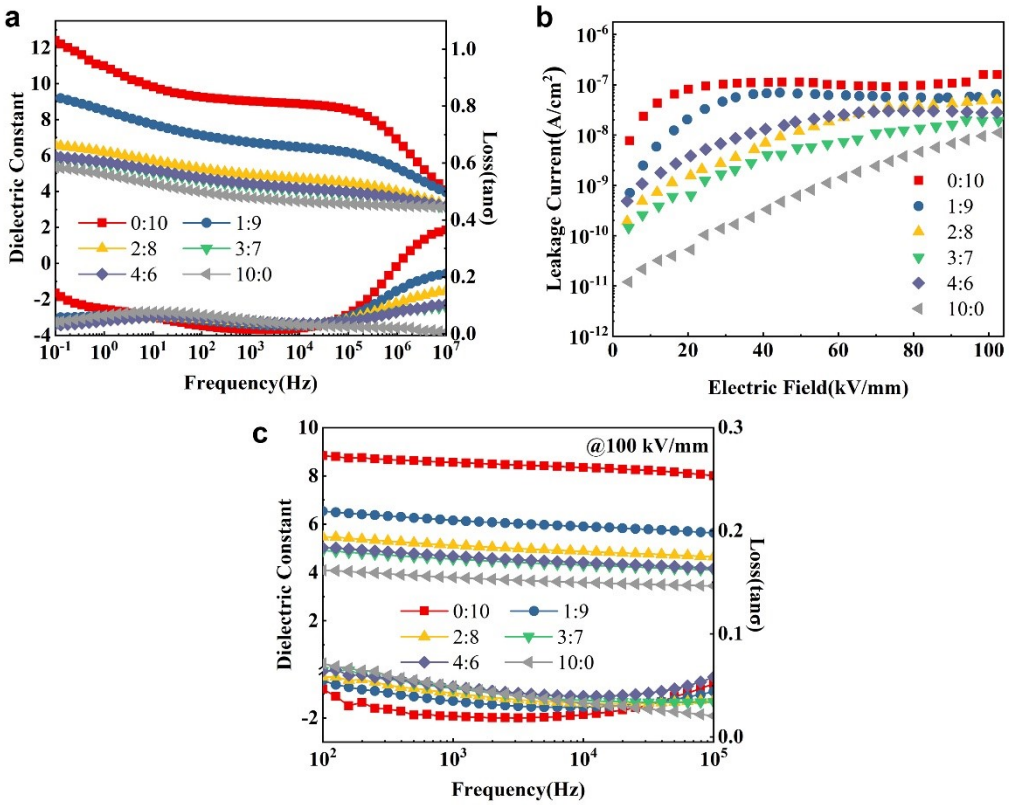

Fig.S4 a) Frequency dependence of dielectric constant and dielectric loss; b) Leakage current; c) The relationship between dielectric constant and dielectric loss and frequency under 100 kV/mm bias field of blend polymers.

Dielectric breakdown under electric field is a complex process, which is affected by field induced breakdown and current induced thermal breakdown. The dielectric breakdown behavior of gradient structure is analyzed by two parameter Weibull distribution function. Weibull equation is described as $P(E)=1-\exp[(E/E_b)^{\beta}]$,[3,4] Where $P(E)$ is cumulative probability of electrical failure, E is experimental breakdown strength, E_b is the characteristic breakdown strength (the scale parameter of breakdown strength when cumulative failure probability is 63.2%), and the shape parameter β is the Weibull modulus, which indicates the divergence of E.

The Weibull distribution of blend polymers is given in Fig.S5a. It can be known that breakdown strength raises with the enhancement of PMMA content. This is because after

introducing linear polymer PMMA into P(VDF-TrFE-CFE), the movement of molecular chains is bound, which reduces crystallinity of P(VDF-TrFE-CFE) and minishes grain size.[5] What's more, PMMA can significantly reduce dielectric constant and electrical conductivity of P(VDF-TrFE-CFE) blend polymers, so it has a positive effect on breakdown strength of P(VDF-TrFE-CFE) blend polymers. It can be known from Fig.S5a that when the volume ratio of PMMA and P(VDF-TrFE-CFE) is 3:7, breakdown strength of blend polymer is the highest, reaching 562.8 kV/mm, 39.2% higher than pure P(VDF-TrFE-CFE) (404.3 kV/mm). To further investigate energy storage capacity of blended polymers, *D-E* loops test were performed, and the results are exhibited in Fig.S5b. Under the same electric field, the maximum electrical displacement decreases with the increasement of PMMA content, which is due to the lower dielectric properties of PMMA. And owning to the augment of linear polymer PMMA content, the residual electrical displacement gradually decreases. Energy storage performance shown in Fig.S5c, breakdown strength and charge-discharge efficiency of blend polymers are greatly improved after introduction of PMMA, and with the enhancement of PMMA content, energy storage density of blend polymers is heightened. Finally, energy density of 14.68 J/cm^3 and efficiency of 78% are obtained at a field strength of 560 kV/mm. The discharge energy density is 98.9% higher than that of P(VDF-TrFE-CFE) (7.38 J/cm^3 at 400 kV/mm). Enhanced energy storage performance can be attributed to huge interaction between PMMA and P(VDF-TrFE-CFE) polymer chains,[5] which leads to suppression of dielectric loss, smaller grain size, limited leakage current density and excellent breakdown strength.

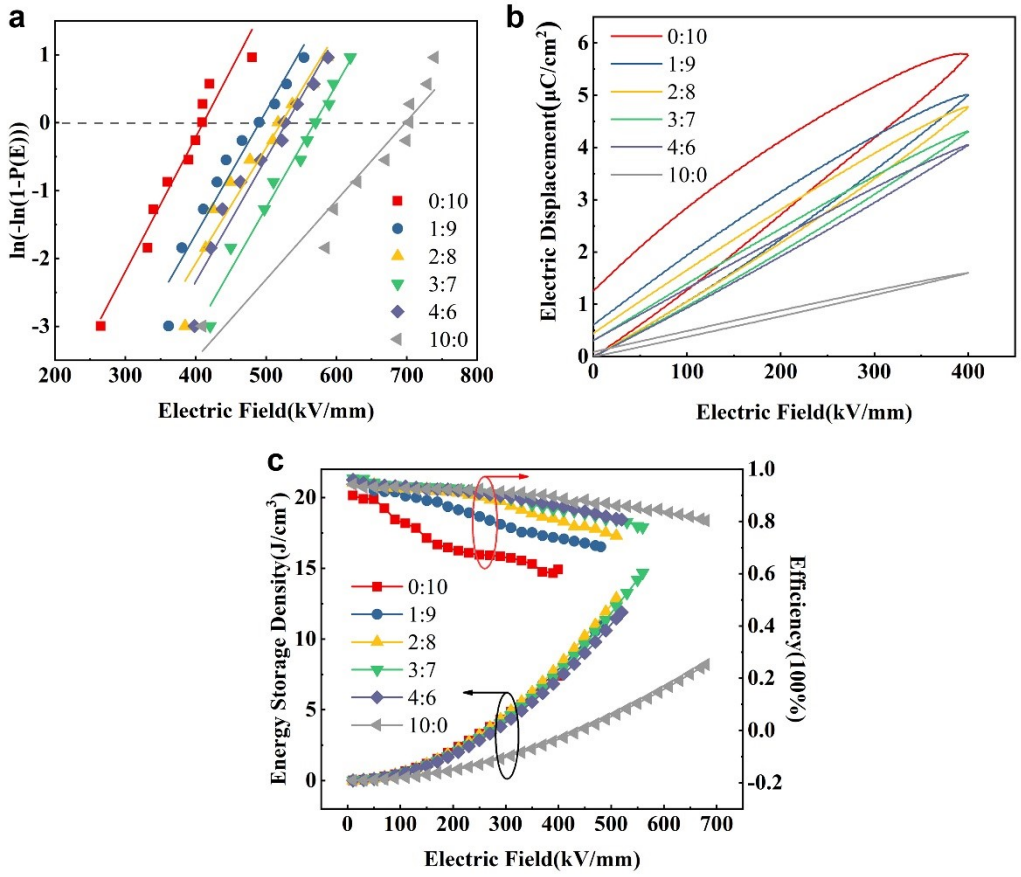

Fig.S5 a) Weibull breakdown strength; b) *D-E* loops; c) Energy storage performance of blend polymers.

Part 2. Two dimensional BNNS doped blend polymer matrix

Hexagonal boron nitride (h-BN) nanosheets are one of the most widely used 2D nanofillers in polymer nanocomposites. The results show that adding thinner boron nitride nanosheets (BNNS) into polymer matrix will amplify barrier height of dielectric/electrode interface, reduce the conductivity and improve breakdown strength as well as thermal properties of composites.

Fig.S6a-d are cross-sectional SEM images of single-layer uniform composite dielectric with 1 vol.%, 2 vol.%, 3 vol.%, 4 vol.% BNNS respectively. The thickness of composite dielectric film is about 14μm. And no obvious air gap and crack are observed, which can determine that the compatibility between inorganic fillers and organic matrix is well. Partially enlarge the cross-sectional images are shown in Fig.S6e-h. It can be seen that the aggregation of BNNS becomes more and more obvious with increase of filling content, which is also the primary reason for deterioration of breakdown strength with high content filling.

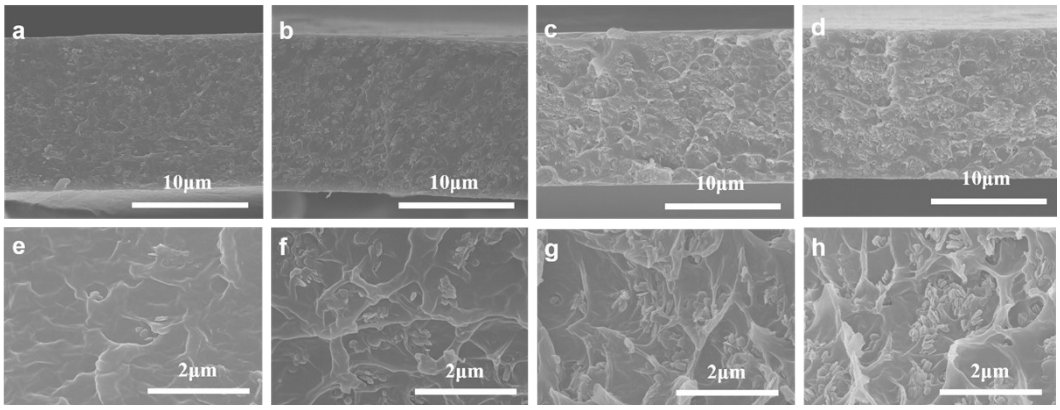

Fig.S6 SEM images of uniform composite dielectric of a)1 vol.% BNNS; b)2 vol.% BNNS; c)3 vol.% BNNS; d)4 vol.% BNNS; e)-h) are the corresponding locally enlarged SEM images.

FTIR spectra in Fig.S7 shows that introduction of BNNS did not vary functional group structure of composite dielectric.

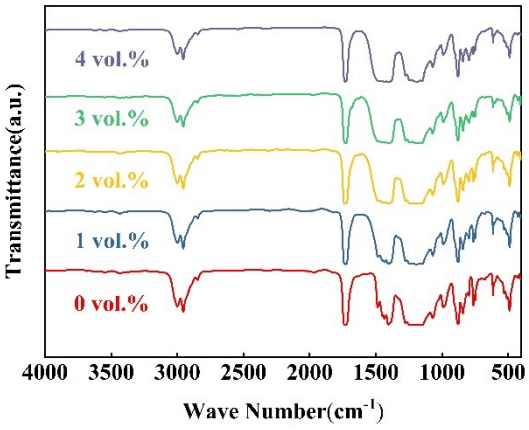

Fig.S7 FTIR spectra of uniform composite dielectric doped with different volume fractions BNNS.

The dielectric constant of polymers decreases with increasing frequency. In general, all composites show similarly trend, which means that the intrinsic chain structure as well as dielectric properties do not change in composites. Fig.S8a shows that dielectric constant of composite dielectric is raised to a certain extent after introduction of BNNS. The higher the doping content is, the greater increasement in dielectric constant is, while dielectric loss keep at low level. A significant decline in dielectric constant and the appearance of dielectric loss peak can be observed around 1 MHz, the special phenomenon attributed to dielectric relaxation of PVDF-based polymers.[6] The effect of BNNS on composite dielectric loss is also reflected in leakage current test. When BNNS, which is more insulating than polymer matrix, is placed near dielectric/electrode interface, the height of charge injection barrier may be elevated, resulting in lower leakage currents than pure films. In Fig.S8b, when BNNS doping content is 1 vol.%, leakage current density is the lowest. This is because BNNS hinders the injection and movement of carriers as well as the formation of conductive paths, so it has better insulation performance and higher breakdown strength. Fig.S8c bias dielectric test results show that dielectric constant and dielectric loss of composite dielectric hold good stability under 100 kV/mm electric field.

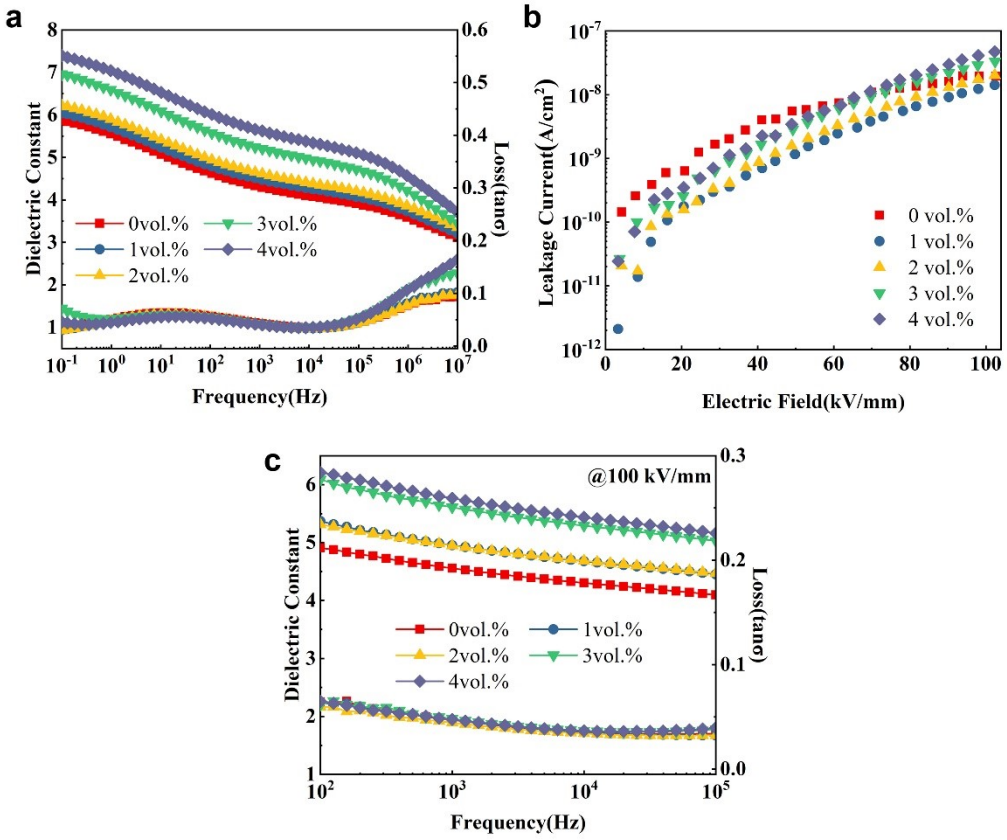

Fig.S8 a) Frequency dependence of dielectric constant and dielectric loss; b) Leakage current; c) The relationship between dielectric constant, dielectric loss and frequency under 100 kV/mm bias field of uniform composite dielectric doped with different volume fractions BNNS.

After introduction of BNNS, the breakdown strength of composite dielectric first raised and then lessened (Fig.S9a). When BNNS content is 1 vol.%, breakdown strength of 63.2% cumulative failure probability is 653.3 kV/mm, which is 1.16 times that of blend matrix. This can be ascribed to BNNS inheriting better insulating properties of layered precursors after exfoliation, enlarging barrier height for electrode charge injection. In addition, during high-speed electrospinning process, 2D BNNS tend to parallel to the in-plane direction of composite dielectric, which can establish effective insulating barrier, augment carrier scattering, limit charge migration, effectively suppress the formation of breakdown paths, and boost breakdown strength of composite dielectric. With further enhance of BNNS amount, the increase of interfaces number

and interfacial area leads to enlarge space charge at interface, and fillers are easily connected with each other, which leads to the damage of composite dielectric breakdown strength. In Fig.S9b, with add of BNNS content, the energy storage density and charge-discharge efficiency of composite dielectric both go up first and then go down. When BNNS amount is 1 vol.%, composite dielectric gets maximum discharge energy density of 17.74 J/cm^3 and efficiency of 78% at 650 kV/mm. The high breakdown strength of composites is prime reason for significant increasement of energy density.

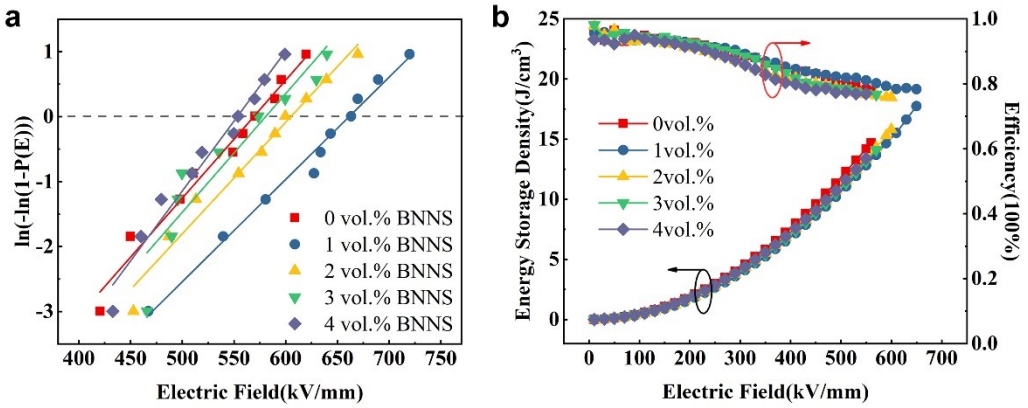

Fig.S9 a) Weibull breakdown strength; b) Energy storage performance of uniform composite dielectric doped with different volume fraction BNNS.

Part 3. Two dimensional TiO_2 doped blend polymer matrix

Fig.S10a-d are the cross-sectional SEM images of single-layer uniform composite dielectric with 1wt%, 3wt%, 5wt%, 7wt%TiO_2 respectively. It can be observed from figure that the thickness of composite dielectric film is about 13~14μm. Partially enlarge cross-sectional images are shown in Fig.S10e-h. It can be observed that TiO_2 aggregation becomes more and more obvious with the augment of filling content, which is also the main reason for deterioration of breakdown strength with high content filling.

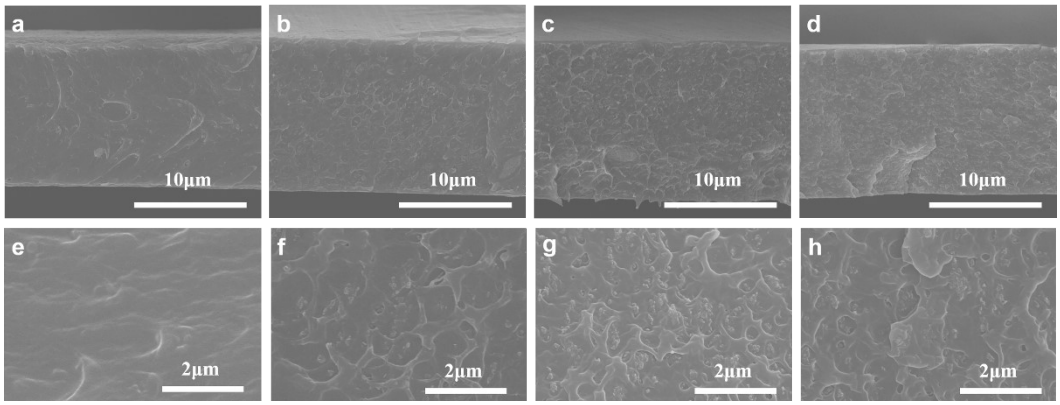

Fig.S10. SEM images of uniform composite dielectric of a) 1wt%TiO_2; b) 3wt%TiO_2; c) 5wt%TiO_2; d) 7wt%TiO_2; e)-h) are the corresponding locally enlarged SEM images.

As shown in Fig.S11, FTIR spectra showed that introduction of TiO_2 into blend matrix did not change the functional group structure of polymer.

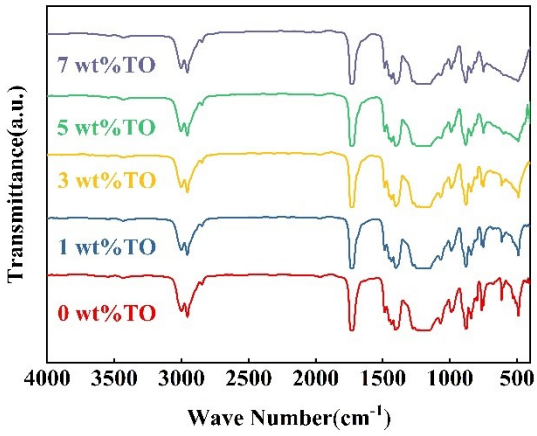

Fig.S11. FTIR spectra of uniform composite dielectric doped with different mass fraction TiO_2.

The relationship curve between dielectric constant, dielectric loss and frequency is given in Fig.S12a. Compared with polymer matrix, introduction of TiO_2 can significantly boost dielectric constant. For example, dielectric constants of 1wt%、3wt%、5wt%、7wt%TiO_2 uniform composite dielectric are 4.98、6.3、6.76 and 7.5 respectively at 10 Hz. Dielectric constant of composite dielectric reduces with the increase of frequency, which may be due to the relaxation phenomenon of the composite dielectric at high frequency. Inevitably, because of introduction TiO_2, the dielectric loss of composite is slightly higher than that of matrix. However, the dielectric loss of composite dielectric remains low level in whole frequency range (at 1 kHz, dielectric loss is less than 0.05). The leakage current test (Fig.S12b) shows that compared with polymer matrix, conduction loss of doped TiO_2 composite dielectric grows with augment of filling content, the change trend is similar to that of dielectric loss. This is because when a large amount of high dielectric constant filler is close to the surface of composite film, it is easy to form breakdown path network, which adds the leakage current and reduces E_b. Under a bias field of 100 kV/mm, both dielectric constant and dielectric loss of composite dielectric maintain good stability, as displayed in Fig.S12c.

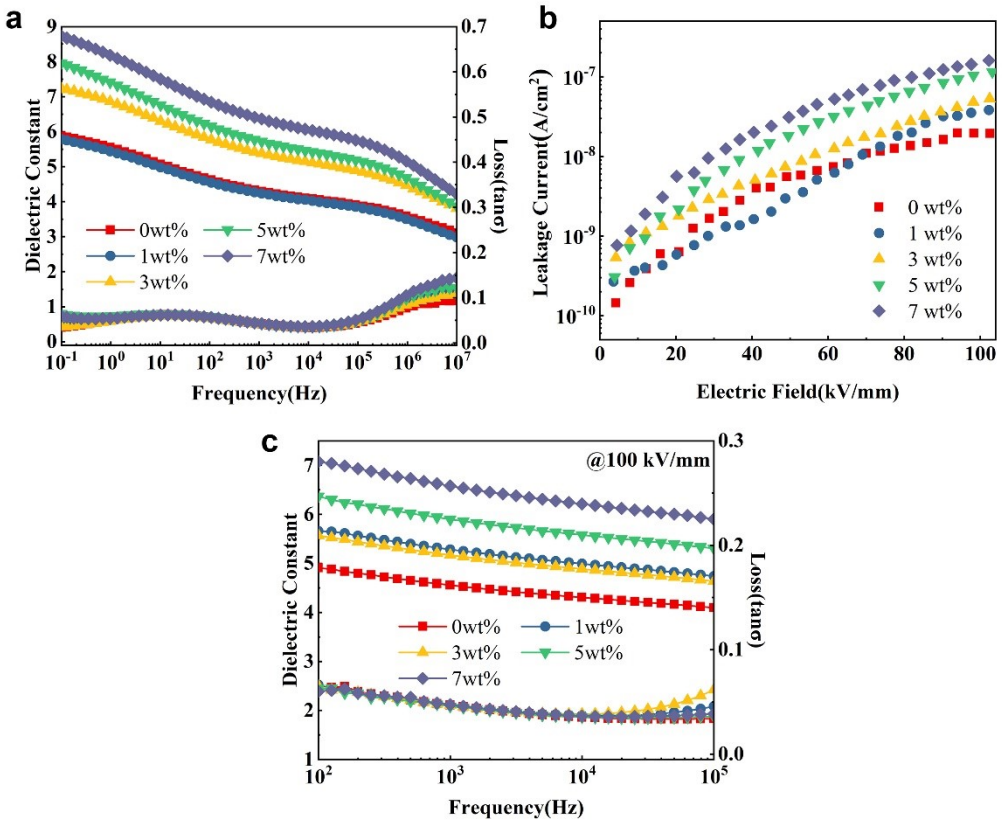

Fig.S12. a) Frequency dependence of dielectric constant and dielectric loss; b) Leakage current; c) The relationship between dielectric constant, dielectric loss and frequency under 100kV/mm bias field of uniform composite dielectrics doped with different mass fractions of TiO_2.

Fig.S13a shows that doping a small amount of TiO_2 can bring about augment of breakdown strength, and the maximum breakdown strength is obtained at 1wt% content. However, from the perspective of TiO_2 as subsequent polarization layer, 3wt%TiO_2 component with the same breakdown as matrix and significantly improved dielectric constant and polarization intensity is selected as the best polarization layer. Due to improvement of polarization intensity, the energy storage density of 3wt%TiO_2 component is 15.56 J/cm^3 and efficiency is 76% at 570 kV/mm.

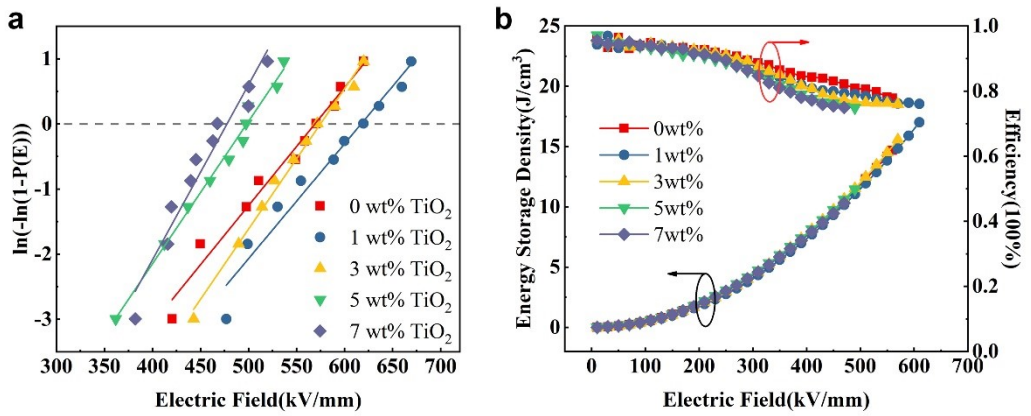

Fig.S13. a) Weibull breakdown strength; b) Energy storage performance of uniform composite dielectric doped with different mass fraction TiO_2.

Part 4. Double gradient composite dielectric

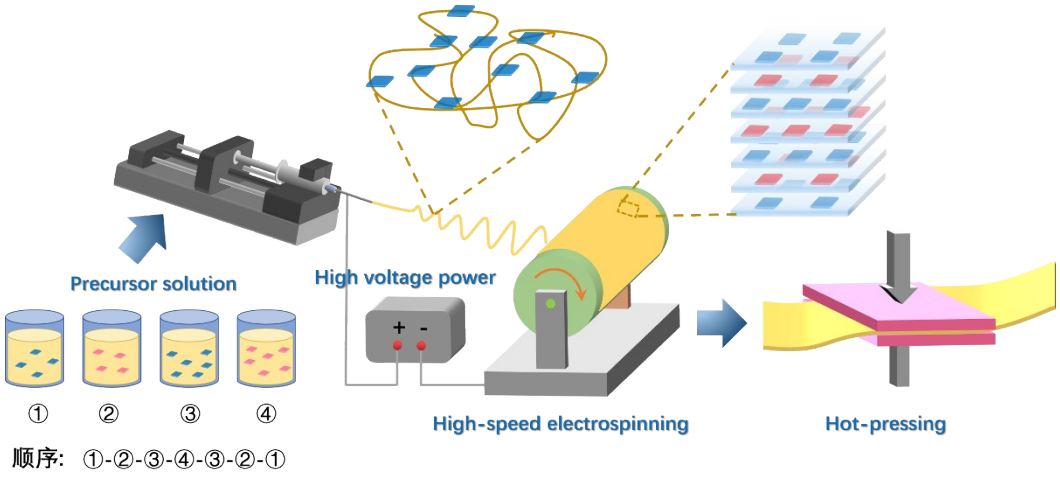

Fig.S14 Schematic diagram of preparing PBPT double gradient composite dielectric.

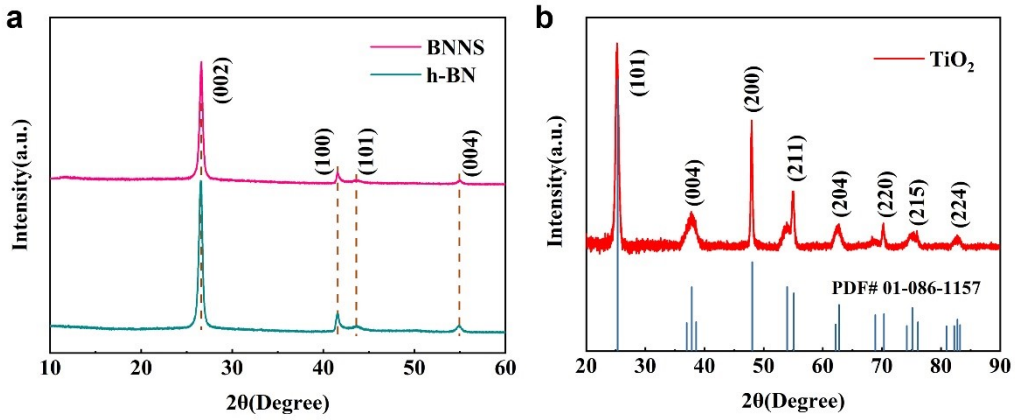

Fig.S15 a) The XRD pattern of h-BN and BNNS; b) The XRD pattern of TiO_2.

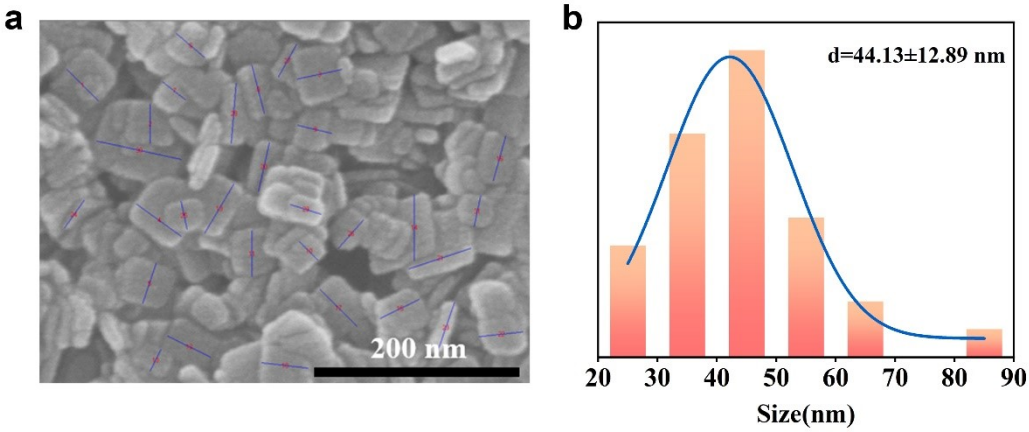

Fig.S16 a) The SEM image of TiO_2; b) Size distribution statistical fitting of TiO_2 nanosheets.

The XRD patterns of PBPT composite dielectric with different fillers gradient spans are

shown in Fig.S17a. The characteristic diffraction peaks of composites are marked in figure. It can be seen that the position and intensity of diffraction peak are almost unchanged, indicating that when fillers overall content is the same, adjusting gradient span distribution of fillers will not change the intensity of diffraction peak. Similarly, the XRD patterns of IBPT composites dielectric also shows the same regularity, as shown in Fig.S17b.

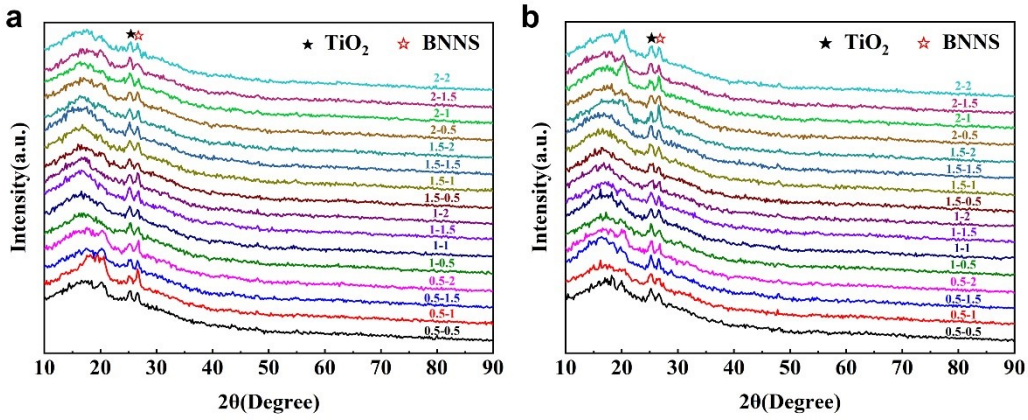

Fig.S17 XRD patterns of a) PBPT; b) IBPT double gradient composite dielectric.

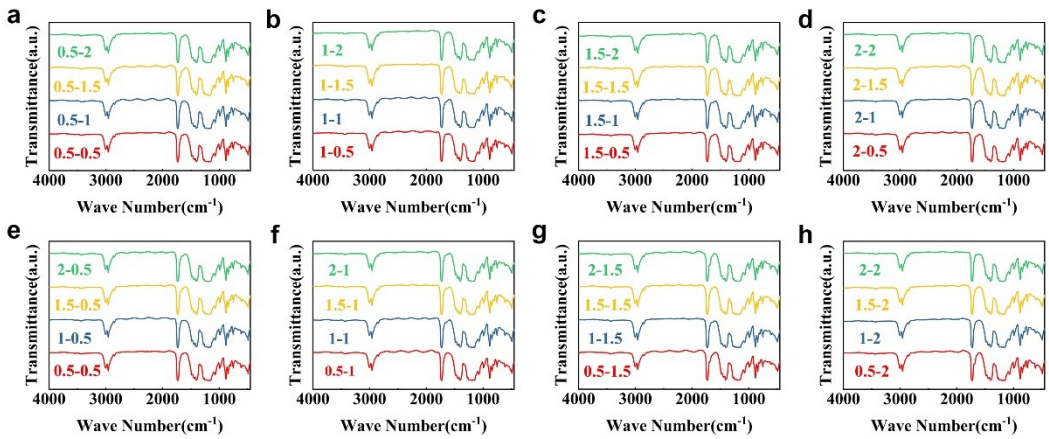

Fig.S18 FTIR spectra of PBPT double gradient composite dielectric.

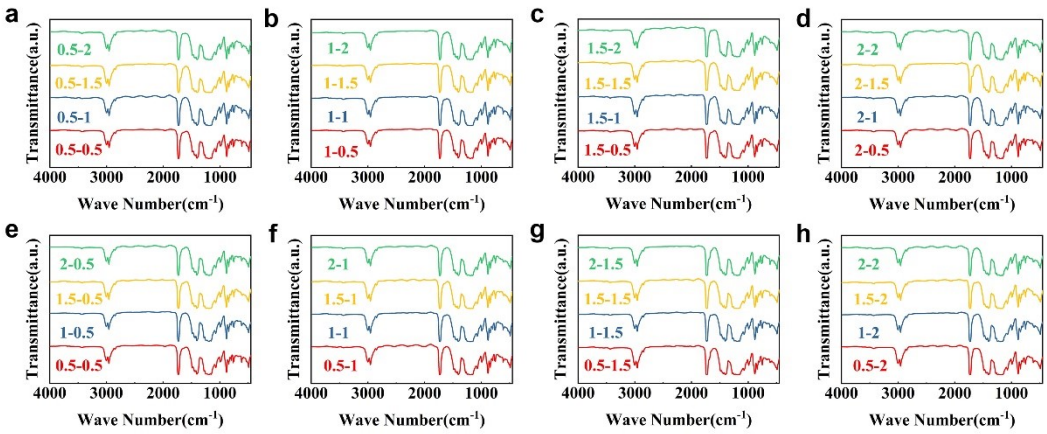

Fig.S19 FTIR spectra of IBPT double gradient composite dielectric.

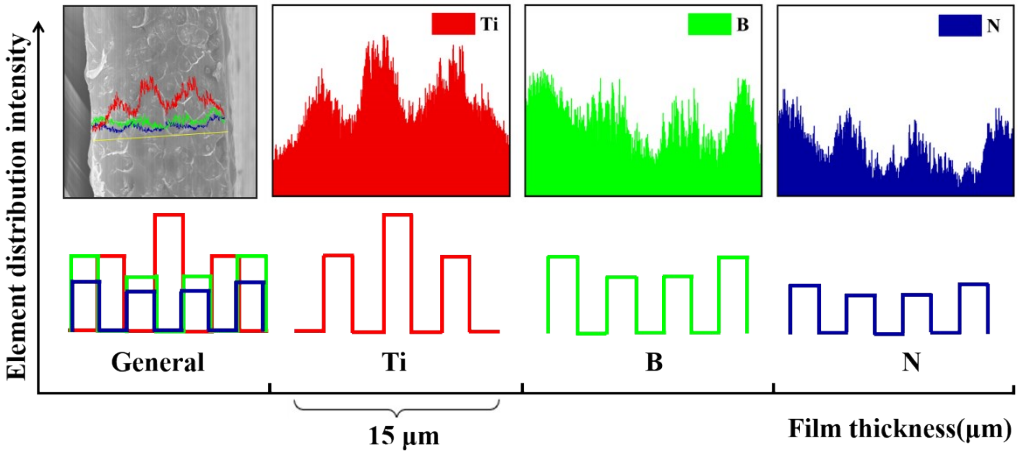

Fig.S20 Element line scanning and ideal schematic diagram of IBPT0.5-2 double gradient composite dielectric.

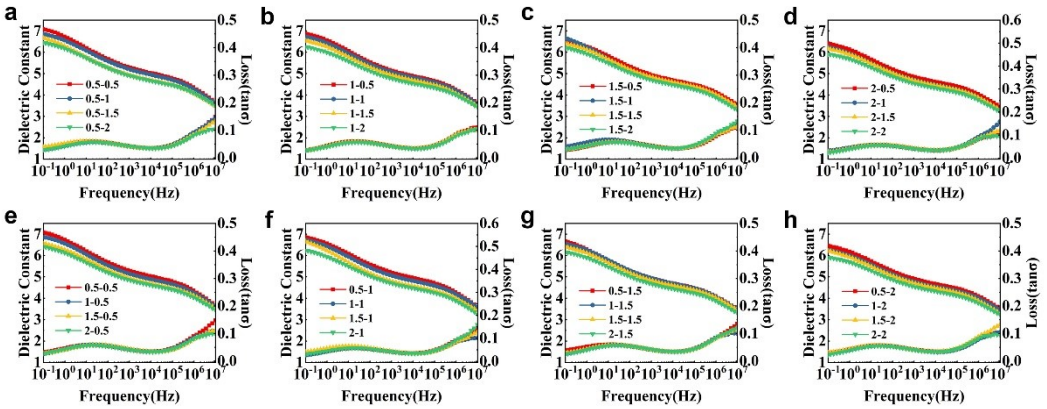

Fig.S21 Dielectric constant and dielectric loss of PBPT double gradient composite dielectric.

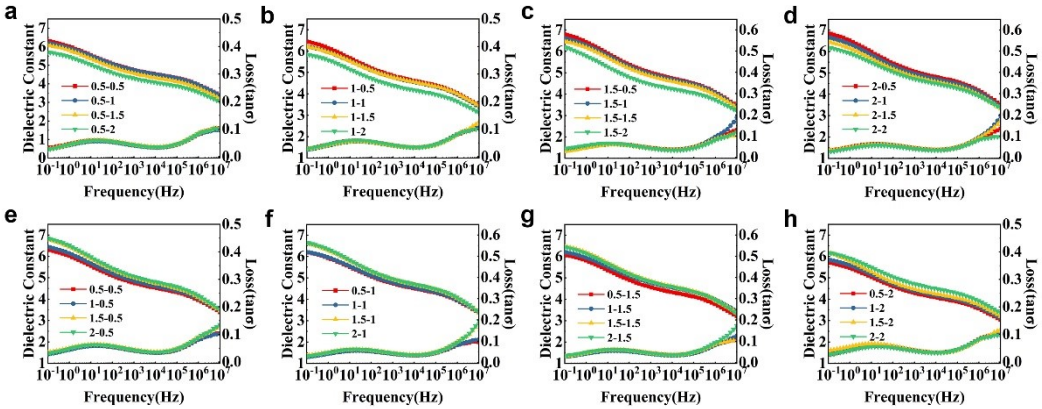

Fig.S22 Dielectric constant and dielectric loss of IBPT double gradient composite dielectric.

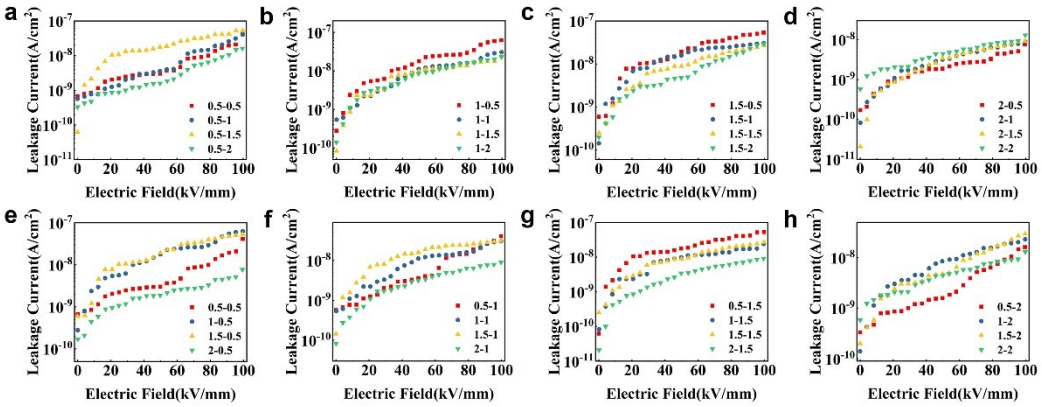

Fig.S23 Leakage current density of PBPT double gradient composite dielectric.

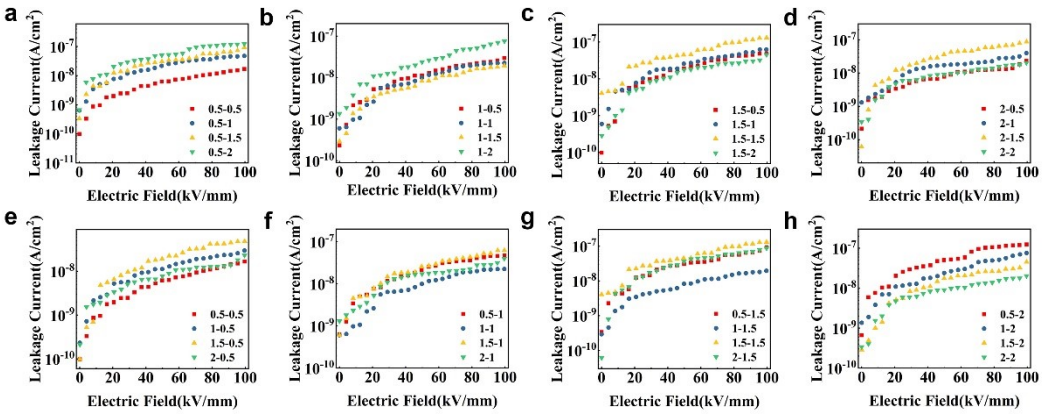

Fig.S24 Leakage current density of IBPT double gradient composite dielectric.

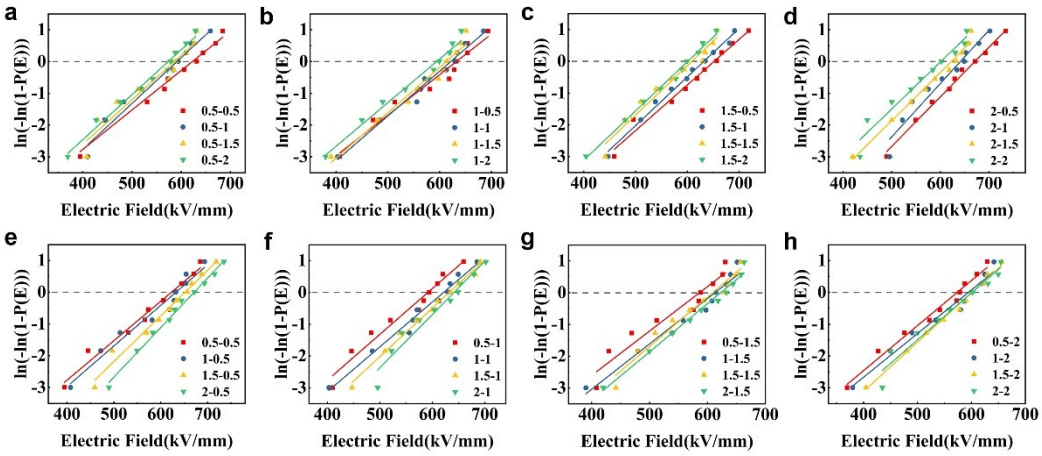

Fig.S25 Weibull breakdown diagram of PBPT double gradient composite dielectric.

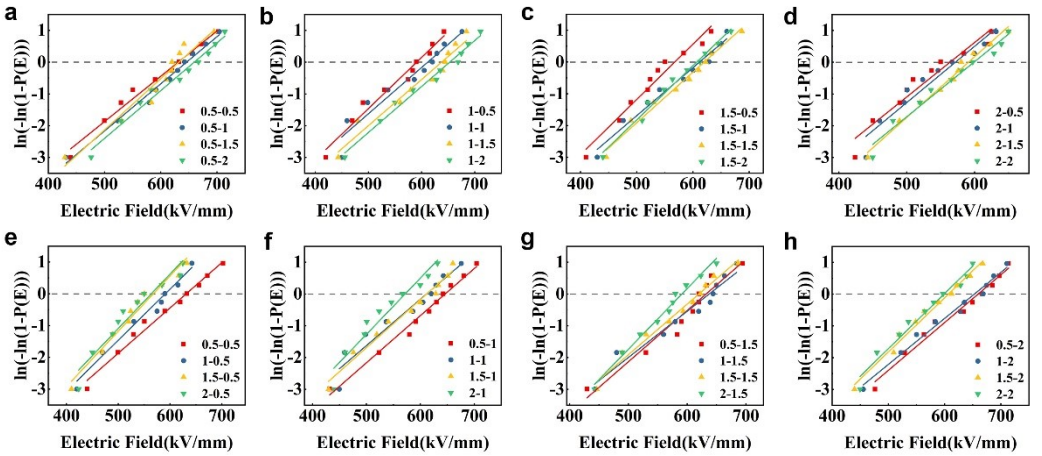

Fig.S26 Weibull breakdown diagram of IBPT double gradient composite dielectric.

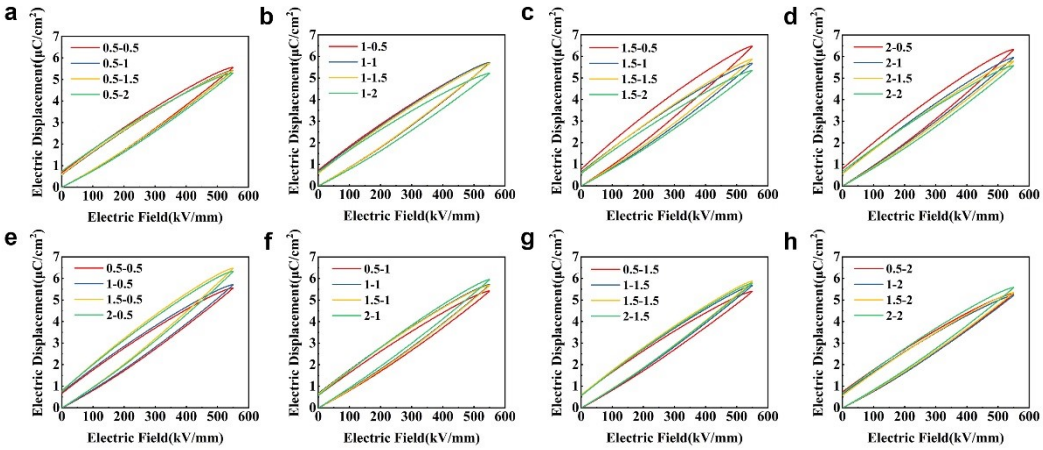

Fig.S27 *D-E* loops of PBPT double gradient composite dielectric.

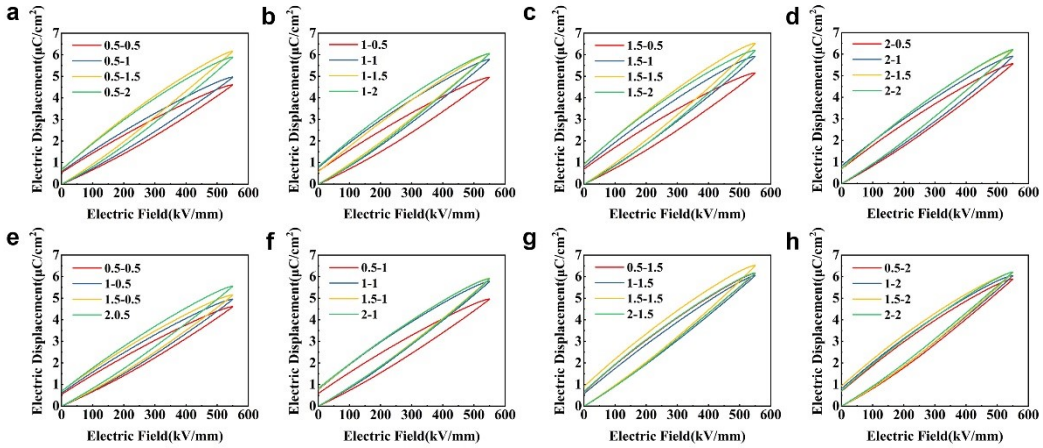

Fig.S28 *D-E* loops of IBPT double gradient composite dielectric.

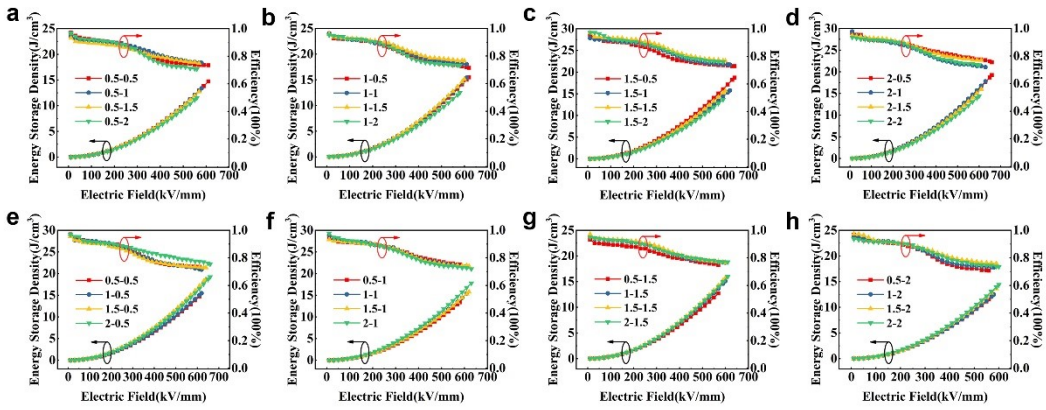

Fig.S29 Energy storage performance of PBPT double gradient composite dielectric.

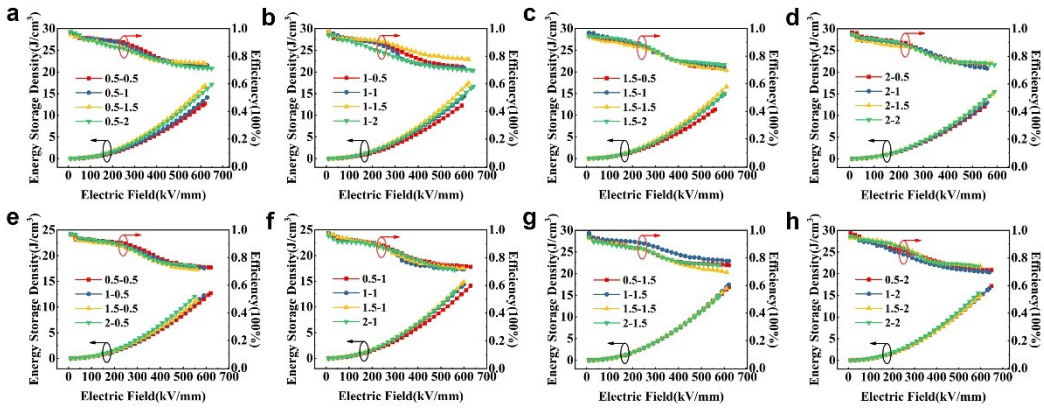

Fig.S30 Energy storage performance of IBPT double gradient composite dielectric.

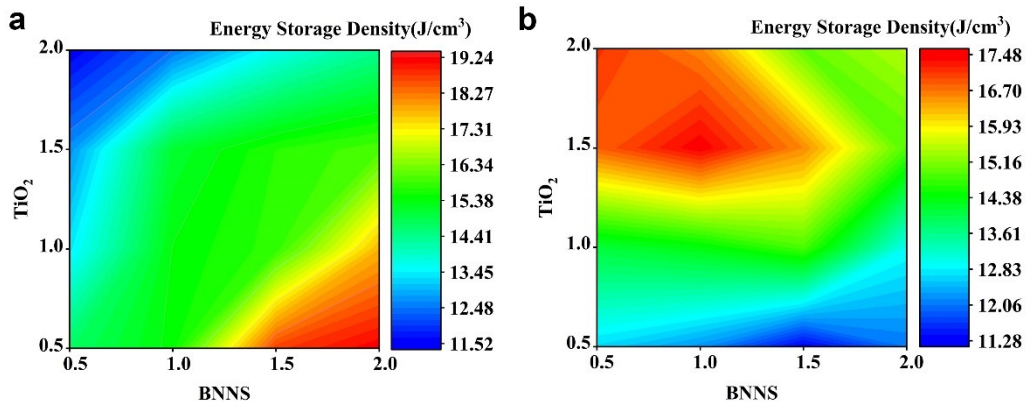

Fig.S31 Discharge energy density contour maps of a) PBPT and b) IBPT double gradient composite dielectric.

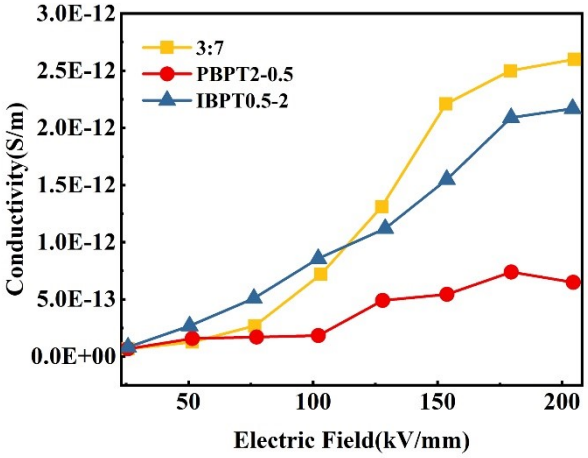

Fig.S32 High field conductivity of 3:7 blend polymer, PBPT and IBPT composite dielectric.

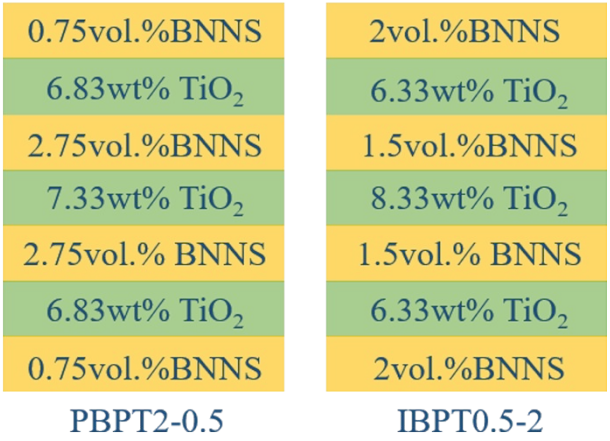

Fig.S33 Filler type and content distribution in each layer of PBPT2-0.5 and IBPT0.5-2 double gradient composite dielectric.

As shown in Fig.S34a, the maximum fluctuation range of discharge energy density of PBPT 2-0.5 and IBPT0.5-2 films is less than 3% of their initial value. In terms of efficiency, compared with PBPT, the efficiency fluctuation range of IBPT during the cycles is slightly larger, but it still does not exceed 4%, and the overall efficiency remains around 89%. In addition, rapid charge-discharge tests were carried out for composite films. Firstly, the dielectric film is quickly charged under the electric field of 200 kV/mm, and then discharged through a 10 kΩ resistance. The time marked in Fig.S34b is the time required to release 95% maximum energy density, and then the power density is further calculated according to the measured energy density and discharge time. The composites prepared in this paper have excellent power density, which is about 4.9 times that of BOPP.

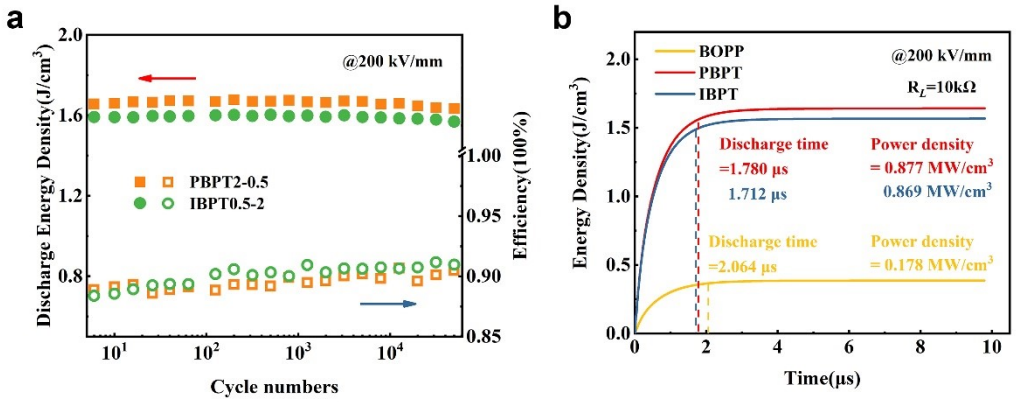

Fig.S34 a) Cyclic stability of energy density and efficiency of composite dielectric; b) Discharge energy density of double gradient composite dielectric and BOPP film under 200 kV/mm electric field and 10 kΩ resistance.

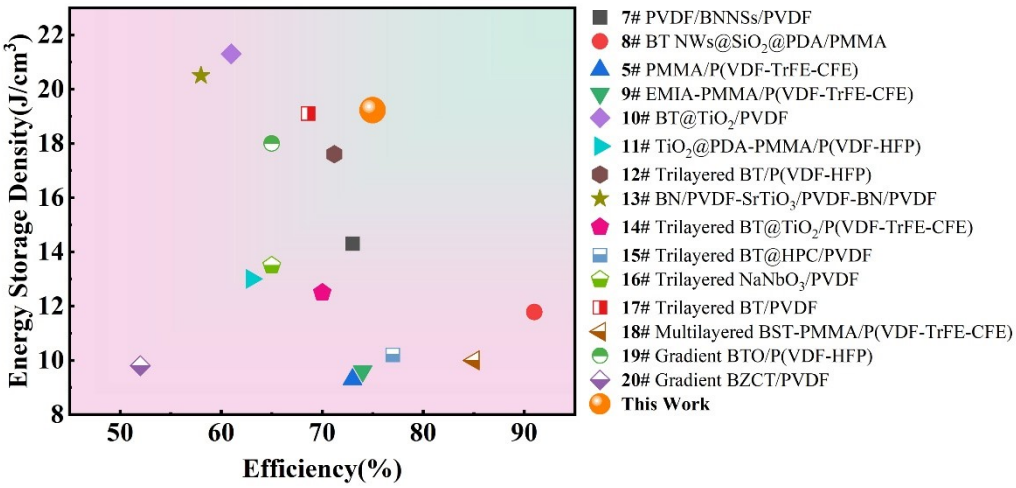

Fig.S35 Comparison of energy storage density and efficiency in PBPT2-0.5 and some typical composites reported in literatures.

References

[1] S. W. Choi, S. M. Jo, W. S. Lee, and Y. R. Kim, *Adv. Mater.*, 2003, **15**, 2027-2032.

[2] Y. Cui, Y. Feng, T. D. Zhang, C. H. Zhang, Q. G. Chi, Y. Q. Zhang, X. Wang, Q. G. Chen, and Q. Q. Lei, *ACS Appl. Mater. Interfaces*, 2020, **12**, 56424-56434.

[3] X. Zhang, J. Y. Jiang, Z. H. Shen, Z. K. Dan, M. Li, Y. H. Lin, C. W. Nan, L. Q. Chen, and Y. Shen, *Adv. Mater.*, 2018, **30**, 1707269.

[4] H. Palneedi, M. Peddigari, G. T. Hwang, D. Y. Jeong, and J. G. Ryu, *Adv. Funct. Mater.*, 2018, **28**, 1803665.

[5] Y. K. Zhu, P. K. Jiang, and X. Y. Huang, *Compos. Sci. Technol*., 2019, **179**, 115-124.

[6] S. Chen, K. Yao, F. E. H. Tay, and C. L. J. Liow, *Appl. Phys*., 2007, **102**, 104108.

[7] Y. K. Zhu, Y. J. Zhu, X. Y. Huang, J. Chen, Q. Li, J. L. He, and P. K. Jiang, *Adv. Energy Mater.*, 2019, **9**, 1901826.

[8] B. Xie, Q. Wang, Q. Zhang, Z. Y. Liu, J. S. Lu, H. B. Zhang, and S. L. Jiang, *ACS Appl. Mater. Interfaces*, 2021, **13**, 27382-27391.

[9] J. Wang, Y. C. Xie, J. J. Liu, Z. C. Zhang, and Y. F. Zhang, *Appl. Surf. Sci*., 2019, **469**, 437-445.

[10] G. Jian, Y. Jiao, L. Feng, Q. Z. Meng, N. Yang, S. T. Zhu, M. F. Lu, and C. P. Wong, *NPG Asia Mater*., 2022, **14**.

[11] Y. K. Zhu, H. Yao, P. K. Jiang, J. D. Wu, X. Zhu, and X. Y. Huang, *J. Phys. Chem. C*, 2018, **122**, 18282-18293.

[12] Y. F. Wang, Y. Li, L. X. Wang, Q. B. Yuan, J. Chen, Y. J. Niu, X. W. Xu, Q. Wang, and H. Wang, *Energy Stor. Mater*., 2020, **24**, 626-634.

[13] F. H. Liu, Q. Li, J. Cui, Z. Y. Li, G. Yang, Y. Liu, L. J. Dong, C. X. Xiong, H. Wang, and Q. Wang, *Adv. Funct. Mater*., 2017, **27**, 1606292.

[14] Y. Shen, D. S. Shen, X. Zhang, J. Y. Jiang, Z. K. Dan, Y. Song, Y. H. Lin, M. Li, and C. W. Nan, *J. Mater. Chem. A*, 2016, **4**, 8359-8365.

[15] X. W. Liang, X. C. Yu, L. L. Lv, T. Zhao, S. B. Luo, S. H. Yu, R. Sun, C. P. Wong, and P. L. Zhu, *Nano Energy*, 2020, **68**, 104351.

[16] Z. B. Pan, B. H. Liu, J. W. Zhai, L. M. Yao, K. Yang, and B. Shen, *Nano Energy*, 2017, **40**, 587-595.

[17] R. Guo, H. Luo, M. Y. Yan, X. F. Zhou, K. C. Zhou, and D. Zhang, *Nano Energy*, 2021, **79**, 105412.

[18] M. J. Feng, Q. G. Chi, Y. Feng, Y. Zhang, T. D. Zhang, C. H. Zhang, Q. G. Chen, and Q. Q. Lei, *Compos. B. Eng*., 2020, **198**, 108206.

[19] Y. D. Jiang, X. Zhang, Z. H. Shen, X. H. Li, J. J. Yan, B. W. Li, and C. W. Nan, *Adv. Funct. Mater.*, 2020, **30**, 1906112.

[20] Y. Zhang, Q. G. Chi, L. Z. Liu, T. D. Zhang, C. H. Zhang, Q. G. Chen, X. Wang, and Q. Q. Lei, *ACS Appl. Energy Mater*., 2018, **1**, 6320-6329.